Monthly Notices
of the
ROYAL ASTRONOMICAL SOCIETY

MNRAS **452,** L31–L35 (2015) doi:10.1093/mnrasl/slv082

Revisiting the dynamical case for a massive black hole in IC10 X-1

Silas G. T. Laycock,[1⋆] Thomas J. Maccarone[2] and Dimitris M. Christodoulou[3]

[1]*Department of Physics, University of Massachusetts Lowell, MA 01854, USA*
[2]*Department of Physics, Texas Tech University, Lubbock, TX 79409, USA*
[3]*Department of Mathematical Sciences, University of Massachusetts Lowell, MA 01854, USA*

Accepted 2015 June 11. Received 2015 June 11; in original form 2015 March 27

ABSTRACT

The relative phasing of the X-ray eclipse ephemeris and optical radial velocity (RV) curve for the X-ray binary IC10 X-1 suggests that the He [λ4686] emission line originates in a shadowed sector of the stellar wind that avoids ionization by X-rays from the compact object. The line attains maximum blueshift when the wind is directly towards us at mid X-ray eclipse, as is also seen in Cygnus X-3. If the RV curve is unrelated to stellar motion, evidence for a massive black hole (BH) evaporates because the mass function of the binary is unknown. The reported X-ray luminosity, spectrum, slow QPO and broad eclipses caused by absorption/scattering in the Wolf–Rayet (WR) wind are all consistent with either a low-stellar-mass BH or a neutron star (NS). For an NS, the centre of mass lies inside the WR envelope whose motion is then far below the observed 370 km s^{-1} RV amplitude, while the velocity of the compact object is as high as 600 km s^{-1}. The resulting 0.4 per cent Doppler variation of X-ray spectral lines could be confirmed by missions in development. These arguments also apply to other putative BH binaries whose RV and eclipse curves are not yet phase-connected. Theories of BH formation and predicted rates of gravitational wave sources may need revision.

Key words: accretion, accretion discs – black hole physics – circumstellar matter – stars: neutron – X-rays: binaries.

1 INTRODUCTION

IC10 X-1 is a high-mass X-ray binary (HMXB) containing a compact object that accretes at $L_X > 10^{38}$ erg s^{-1} from the wind of its Wolf–Rayet (WR) companion (Prestwich et al. 2007). The binary period is 35 h and deep eclipses are seen in the X-ray light curve. This Letter addresses the strong doubts cast by the recent observations of Laycock, Cappallo & Moro (2015) on the massive black hole (BH) interpretation for this system. A substantial downward revision of the mass of the compact object will impact research on the evolution of massive stars and BHs of all sizes (Barnard, Clark & Kolb 2008; Carpano et al. 2008; Belczynski, Bulik & Fryer 2010; Park & Ricotti 2011), long gamma-ray bursts and BH–BH sources of gravitational waves (Bulik, Belczynski & Prestwich 2011; Bogomazov 2014), as well as the so-called ultra-luminous X-ray (ULX) sources (Soria 2007; Gladstone, Roberts & Done 2009; Feng & Soria 2011; Medvedev & Putanen 2013). In particular, the noted preference for massive BH candidates to occur in low-metallicity environments would lose its central exemplar.

1.1 High-mass X-ray binaries

Binary systems containing X-ray emitting compact objects accreting matter from their companion stars are thought to host both neutron stars (NSs) and BHs. The compact objects themselves are invisible due to their very small sizes and correspondingly low intrinsic luminosities. Their existence is inferred from the properties of the X-ray emission and from the Doppler-derived motions of the companions as the stars orbit around their centres of mass. Spectral lines originating at the surface of the primary are observed repeatedly over the course of one or more orbital cycles to establish the amplitude of the radial velocity (RV) curve. Tidal distortion of the primary (in close systems) also leads to a periodic optical brightness modulation, known as ellipsoidal variation, which can be seen in the photometric light curve. Modelling of these variations can yield an independent measurement of the orbital period and inclination of the system. Since it is only the primary that is directly observed, the mass function is combined with independent estimates of its mass to constrain the mass of the unseen companion. These techniques have yielded a growing list (e.g. Remillard & McClintock 2006; Casares & Jonker 2014) of binary systems where the compact object mass is significantly above the theoretical limit of 2.9 $M_\odot$ for NSs. Such systems are generally (although not universally) accepted to contain BHs.

⋆ E-mail: silas_laycock@uml.edu

Another class of objects thought to contain stellar-mass BHs are the ULX sources (Liu et al. 2013; Motch et al. 2014). Their X-ray luminosities (10^{39}–10^{41} erg s^{-1}) exceed the Eddington limit for an NS by 1–3 orders of magnitude. Most ULXs are too distant for RV or photometric studies by existing instruments to reveal their dynamical parameters, so the argument for stellar-mass BHs in these systems derives mainly from their X-ray properties.

The X-ray binary (XRB) IC10 X-1 occupies an important niche as a link between BH-HMXBs and ULXs due to its intermediate luminosity ($\sim 10^{38}$erg s^{-1}) and the fact that, at a distance of 660 kpc, it is one of the few extragalactic systems close enough to be readily observable by current-generation telescopes. The landmark work of Silverman & Filippenko (2008) revealed that IC10 X-1 appears to have an RV-derived mass function that requires a BH of 23–32 $M_\odot$. Silverman & Filippenko (2008) noted that their RV curve had not been phase-aligned with the X-ray eclipses since the X-ray period was not then known to sufficient precision. Others (e.g. Tutukov, Fedorova & Cherepashchuk 2013) have pointed out that this caveat also applies to NGC 300 X-1 which is in many regards a twin to IC10 X-1 in terms of its WR companion, similar orbital period and X-ray luminosity.

1.2 Wind ionization and shadowing

In the most massive and hottest stars, the stellar photospheres are highly ionized so that no suitable absorption lines can be found and emission lines are used instead. The most suitable ion species is He II because it can exist at the temperatures found in the photospheres of O stars ($>3 \times 10^4$ K), where it gives rise to the Pickering series of spectral lines. Emission lines arise in low-density gas, so the region probed by the He II lines can in principle extend to many stellar radii above the surface. The density of stellar winds falls with distance r approximately as $1/r^2$, so most of the equivalent width of the line should originate at lower altitudes. Provided that the wind is isotropic (or at least azimuthally symmetric), the He II line should still trace the orbital motion of the star.

At the very high X-ray fluxes seen in high-luminosity XRBs, the wind will be completely ionized out to a distance far exceeding the orbital separation of the binary. This fact has not been generally recognized as affecting the mass determinations obtained via the RV-curve method. Maccarone et al. (2014) have recently pointed out that a model introduced by van Kerkwijk et al. (1996) for Cyg X-3 might apply more widely. In this model, X-ray photoionization of the wind suppresses line emission throughout the binary orbit. Only in a small sector of the wind shielded by the primary will the gas be able to maintain a 'normal' ionization state. In IC10 X-1, the ionization parameter has a large value ($L_X/nd^2 \sim 10^3$) at the location of the WR star (Barnard et al. 2014). The wavelength and shape of the observed emission lines will be a convolution of the wind velocity $v_{\rm wind}$, the orbital motion $v_{\rm orbit}$ and the stellar rotation $v_{\rm rot}$.

In the limit that $v_{\rm wind} \gg v_{\rm orbit}$, $v_{\rm rot}$, the observed RV curve will have an amplitude of $v_{\rm wind} \sin i$, where i is the inclination of the orbital plane to the line of sight. The phase of the resulting RV curve will be as follows: at mid X-ray eclipse, when the WR star lies between us and the X-ray source, the shielded wind sector is pointing towards the observer, as illustrated in Fig. 1. The wind velocity vector then lies along our line of sight, producing the maximum blueshift of the emission line. At quadrature, when the WR star's projected RV is greatest, the wind in the shielded sector is orthogonal to the line of sight, producing zero Doppler shift.

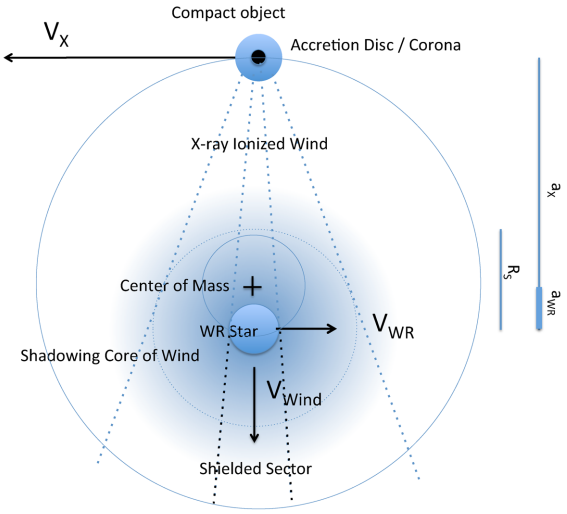

Figure 1. Schematic diagram of the IC10 X-1 system for $M_{\rm WR} = 35$ $R_\odot$ and $M_X = 1.4$–2.5 $M_\odot$ with all components drawn approximately to scale (see Table 1). X-ray eclipses occur as the WR star's dense wind core region passes through the line of sight to the compact object. At mid-eclipse, a 'shielded sector' of the wind that lies in the shadow of the WR star will be pointing directly towards the observer. The vector $v_{\rm wind}$ represents the velocity of the partially ionized material that gives rise to the optical He II emission line. Enhanced absorption and scattering by this cooler material contributes to the depth and shape of the eclipse minimum. The cross represents the centre of mass of the binary. The large mass ratio causes the compact object to move in a wide orbit at high speed while the WR star moves only slightly by comparison. For small M_X, the centre of mass lies inside the WR envelope.

Finally at superior conjunction, the emitting portion of the wind is expanding away from us, leading to the maximum redshift. Hanson, Still & Fender (2000) were able to map this cool structure in Cyg X-3 from IR spectra using Doppler tomography.

The actual phase relationship between X-ray eclipses in IC10 X-1 and the RV curve of the optical counterpart has been recently explored by Laycock et al. (2015). After constructing a new ephemeris for the X-ray eclipses from a 10 year series of *Chandra* and *XMM–Newton* observations, it was found that the published RV data of Silverman & Filippenko (2008) are offset by 1/4 of an orbit from the geometric alignment implied by the eclipses. The phase shift is such that the periodic Doppler shift of the He [λ4686] line does not pass though zero at mid-eclipse. Instead, it is the maximum blueshift that occurs at mid-eclipse which is expected to coincide with inferior conjunction of the WR primary.

Variations in He II line width are evident from table 2 of Silverman & Filippenko (2008), which suggests that the full width at half-maximum is largest when the RV is closest to zero and smallest at maximum redshift. In van Kerkwijk et al. (1996) the line profile model consists of a weak broad contribution from the hot mostly ionized stellar wind, plus a narrow velocity-modulated line from the cool gas in the shadow which alternately passes in front of and behind the star, attaining its minimum width (and greatest strength) at maximum redshift. $v_{\rm wind}$ in the line-forming region is substantially lower than the terminal wind velocity. Vilhu et al. (2009) used *Chandra* HETG spectra to map the ionization and velocity fields of the wind in Cyg X-3, largely confirming the picture developed by van Kerkwijk et al. (1996) and Hanson et al. (2000) and showing that the wind is highly ionized out to many times the binary separation. The X-ray Fe XXVI line RV curve appears to trace the

compact object's motion, with the required phase relationship to the IR emission and absorption features, resulting in a mass function consistent with that obtained by Hanson et al. (2000).

The appeal of the van Kerkwijk et al. (1996) model is that it isolates a single phenomenon (photoionization) that seems likely to dominate interaction in IC10 X-1; it is not unique in producing phase shifts and newer models for Cyg X-3 successfully reproduce many elements of *its* more complex dynamics. The phenomena encompassed by those models probably apply to a lesser extent in IC10 X-1 since the orbital separation in Cyg X-3 is smaller, resulting in the compact object being engulfed by the stellar envelope. The flow of material in that system is influenced by both ionization and tidal interactions, leading to density structures such as plumes, wake trails, and shocks, while IC10 X-1 has so far been observed in a state analogous to the quiescent state of Cyg X-3.

1.3 Spectral analysis of IC10 X-1

IC10 is distant and so grating spectra have not yet been obtained. Wang, Whitaker & Williams (2005) fit the *XMM–Newton* EPIC (pulse height) spectrum with a multicolour disc blackbody model appropriate to a BH in the low hard state. Finding an inner accretion disc temperature of $T_{\rm in} = 1.11^{+0.06}_{-0.05}$ keV at a radius of $R_{\rm in} = 25^{+4}_{-6}$ km, disc inclination angle $>57^{\circ}$, subsolar metal abundance and $N_{\rm H} \sim 10^{22}$ cm^{-2}. The point source is blended with an extended diffuse structure of effective radius of 50^{+23}_{-7} km, which appears to be an ionized X-ray nebula surrounding the compact object. Unfortunately, these early observations did not accumulate enough counts during eclipse to fully isolate the spectral components. By looking at the variation in hardness ratio (HR) during eclipse egress in the *Chandra* data, Laycock et al. (2015) found evidence of energy dependence and noted that the HR increases *before* the flux begins its climb at egress. Energy dependence is not expected in the eclipse profile of an X-ray point source passing behind a fully ionized absorber. The modulation would be dominated by free electron scattering which is energy independent over this wavelength range. At the more moderate ionization fraction expected deep in the core of the wind (and especially in the shadow of the WR star), single-electron ions of e.g. O, C, Si and Fe will be present [as seen by Vilhu et al. 2009 in Cyg X-3] and contribute significant soft X-ray absorption.

A much longer *XMM–Newton* EPIC observation analysed by Barnard et al. (2014) reveals evidence for an accretion disc corona. Their fig. 2 shows a clear HR modulation during eclipse. The interpretation is that different parts of the emission region (disc and corona) become covered by the absorber as the eclipse progresses. They avoid the word eclipse in favour of 'dip' because the passage of the compact object through (and behind) the wind gives rise to varying amounts of scattering and absorption at all phases. Thus, what we call the eclipse is referred to by them as the 'main dip'. The inner-edge temperature for their preferred accretion disc spectral fit (Model V) is $T_{\rm in} = 1.68$ keV, and this component disappears during eclipse, while about 10 per cent of the spatially extended, Comptonized corona component remains visible ('partial covering'). We note that Model V is not the best-fitting model of Barnard et al. (2014). Model III with $T_{\rm in} = 0.2$ keV and a compact corona was a better fit, but was rejected (in part) because it does not conform to the assumption of a (massive) stellar-mass BH. The very large number of parameters required in these models results from the lack of information about the spectrum above 10 keV, and the inability of current data sets to resolve the soft X-ray lines expected from hydrogen-like heavy ions in the absorbing core of the wind.

In what follows, we adopt the model shown in Fig. 1 for optical line emission during X-ray eclipses and in Section 2 we make the case for a low-mass compact object in IC10 X-1, possibly an NS although a low-mass BH cannot be ruled out. In Section 3, we discuss the implications for other HMXBs and ULXs, and in Section 4 we summarize our conclusions.

2 A LOW-MASS COMPACT OBJECT

If we in fact do not know the mass function of IC10 X-1, then the only hard evidence on which to base a model for the system comes from the orbital period and the stellar parameters of the WR primary. The X-ray luminosity and eclipse duration are informative but they are subject to many more parameters (wind density, ionization, accretion efficiency, magnetic field), and consequently they can be used to support competing non-unique solutions. Here we analyse the plausibility of a much lower mass BH or an NS as the compact object.

The mass of the WR star is reasonably well constrained by the optical classification of Clark & Crowther (2004) with a most probable value of $M_{\rm WR} = 35\,{\rm M}_{\odot}$ and a range of 17–35 $\rm M_{\odot}$. For an NS companion, a commonly accepted range for the mass is $M_{\rm NS} = 1.26$–$2.5\,{\rm M}_{\odot}$, where the lower bound is the Chandrasekhar limit for a white dwarf minus the binding energy lost in collapse to an NS, and the upper bound is the Tolman–Oppenheimer–Volkoff limit for an NS. The highest reliable measurement is $2.0\,{\rm M}_{\odot}$ and current EOS allows 0.1–$2.9\,{\rm M}_{\odot}$. For BHs, there are no physical bounds to the mass and any dynamically confirmed object significantly in excess of $2.5\,{\rm M}_{\odot}$ is regarded as a probable BH.

Applying Kepler's law with NS masses yields an orbital separation of $(a_1 + a_2) = 14\,{\rm R}_{\odot}$ for the lowest mass combination ($1.4 + 17\,{\rm M}_{\odot}$) and $19\,{\rm R}_{\odot}$ for the highest mass combination ($2.5 + 35\,{\rm M}_{\odot}$). Naturally, the NS orbit shrinks now to 14–19 $\rm R_{\odot}$ relative to the 19–23 $\rm R_{\odot}$ range used in prior investigations that assumed a 23–32 $\rm M_{\odot}$ BH (see Table 1). At these closer separations, the stellar wind density encountered by the compact object increases and the primary approaches filling its Roche lobe. The size of the Roche lobe of the primary for all of these combinations of WR star and NS masses is $r_1 \approx 0.6(a_1 + a_2) = 8$–$11\,{\rm R}_{\odot}$.

Analyses of the *Chandra* and *XMM–Newton* eclipse profiles by Laycock et al. (2015) and Barnard et al. (2014), respectively, measured slightly different durations for minimum flux (5 h versus 5.2 h) and ingress/egress phases ($\sim$1 h versus $\sim$2 h). This appears to be due to the broader and more gradual eclipse seen by *XMM–Newton*. Differences in the method used to estimate the diameter of the WR star also led to small variations in the estimates of the size of the eclipsing body (4 versus 5 for $R_{\rm WR}$). Barnard et al. (2014) estimated

Table 1. Orbital Parameters for an NS or a BH in IC10 X-1.

$M_{\rm WR}$ ($\rm M_{\odot}$)	$M_{\rm X}$ ($\rm M_{\odot}$)	a ($\rm R_{\odot}$)	$v_{\rm WR}$ (km s^{-1})	$v_{\rm X}$ (km s^{-1})	R(s) ($\rm R_{\odot}$)	$R_{\rm WR}$ ($\rm R_{\odot}$)	$T_{\rm WR}$ (h)
35	1.4	18.99	23.96	599.10	8.06	2	1.24
35	2.5	19.18	41.95	587.32	8.14	2	1.23
17	1.4	15.13	37.76	458.57	6.42	1.5	1.17
17	2.5	15.42	64.88	441.15	6.55	1.5	1.15
35	32	23.27	364.7	398.9	9.88	2	1.01
17	23	19.59	369.7	273.3	8.32	1.5	0.90

Notes. Radius of shadowing body R(s) determined from observed eclipse duration $T_{\rm min} = 5$ h. Inferred duration for eclipse by the WR star is $T_{\rm WR}$. This table assumes inclination $i = 90^{\circ}$.

the effective stellar radius $R_{\rm WR}$ seen by the X-rays to be the blackbody radius implied by the colour temperature reported by Clark & Crowther (2004), while we used the tabulated WR mass–radius relation of Langer (1989) which produces slightly smaller results.

In the case of an NS secondary, the orbital separation does not shrink enough to cast doubt on the results of Barnard et al. (2014) and Laycock et al. (2015) in regard to the general size of the shadowing absorber and the extended corona. The binary separation and the orbital velocities change together, so that the sizes inferred from eclipse timing remain relatively unchanged; Table 1 shows a contraction of about 20 per cent. The eclipse is still several times larger than can be explained by an eclipse of the WR star. Hence, the X-ray flux modulation is still required to be dominated by absorption and scattering in the dense core of the stellar wind, perhaps in the cooler shadowed material (Fig. 1).

The parameter that changes most dramatically is the orbital velocity of the WR star $v_{\rm WR}$, which decreases by a factor of ∼10–15 for $M_{\rm X} = 1.4\,{\rm M}_{\odot}$ (Table 1). An important consequence is that now $v_{\rm wind} \gg v_{\rm WR}$ which is a requirement for the van Kerkwijk et al. (1996) model to be valid. Then the observed RV curve is expected to reflect only a small advance in phase due to the orbital and rotational velocities of the WR star that are both very small compared to $v_{\rm wind}$. The complete picture is more complicated: at increasing distances r from the WR star, the shielded sector contains material that was ejected earlier from the point of view of an observer corotating in the shadow (Fig. 1). So, as the wind expands outwards, its tangential velocity (fixed at the stellar surface value $v_{\rm rot}$) is rapidly outpaced by the motion of the shadow whose velocity goes as $r\omega$. Thus, the projected velocity of the emission line will be influenced by the phase advance provided by the stellar surface velocity and the trailing which becomes larger at higher altitudes. The result will be a line profile that depends on the viewing angle and hence on orbital phase. A constant centre of mass or γ velocity is expected in the RV curve; this is not evident in Silverman & Filippenko (2008) who measured their line centroids relative to nebular lines, which probably comove with the binary. In Cyg X-3, γ has not been measured in optical/IR spectra despite that system having a large X-ray derived value, a situation Hanson et al. (2000) attribute to turbulence.

Model calculations for IC10 X-1 by Tutukov et al. (2013) found that for accepted values of the stellar wind parameters in WR stars, the X-ray source should have been more luminous by at least one order of magnitude. A similar conclusion was reached by Barnard et al. (2014), that a mere 2 per cent of the Bondi accretion rate is sufficient to power the observed X-rays. Both of these calculations assumed large BH masses; however, an adopted lower mass (permitted by our reinterpretation of the dynamical data) eliminates the discrepancy. Specifically, for typical NS parameters ($M_{\rm X} = 1.4\,{\rm M}_{\odot}$ and $R_{\rm X} = 10$ km) and for the measured dynamical parameters ($M_{\rm WR} = 35\,{\rm M}_{\odot}$, $P_{\rm orbit} = 1.45$ d and $v_{\rm wind} = 370$ km s^{-1}), we find from equation 4 of Stella, White & Rosner (1986) for direct wind accretion that $L_{\rm X} = 1.5 \times 10^{38}$ erg s^{-1} when we also adopt the value of $\dot{M} = 2.6 \times 10^{-7}\,{\rm M}_{\odot}\,{\rm yr}^{-1}$ proposed by Tutukov et al. (2013) for the rate of the mass captured by the accretor.

3 DISCUSSION

As a putative 24 $\rm M_{\odot}$ BH with a 35 $\rm M_{\odot}$ companion located in a low-metallicity ($Z = 0.3\,{\rm Z}_{\odot}$) galaxy, IC10 X-1 has contributed to the picture of metallicity as determining maximum stellar BH mass. Dynamically confirmed BHs are few in number, so it is striking that the most massive, including ULX BHs, and intermediate-mass (IMBH) candidates (e.g. HLX-1 in ESO 243-49; Farrell et al. 2014) have been found in galaxies with extremely low Z. Detailed stellar evolution calculations (Belczynski et al. 2010) show that metallicity determines the mass-loss rate in the progenitor star's wind and hence the remnant mass. The feasibility of IMBHs growing in cluster or galaxy cores from stellar BH 'seeds' via dynamical interactions is critically sensitive to the initial stellar BH mass. The above is no longer supported by IC10 X-1 if the compact object has a low mass.

The debate about the nature of the compact objects in ULXs (e.g. Gilfanov, Grimm & Sunyaev 2004; Luangtip et al. 2014) continues to this day as new observations arise, and the balance has tipped recently in favour of stellar-mass BHs and NSs (M101 ULX-1, Liu et al. 2013; M-82 X-2, Bachetti et al. 2014; NGC 7793 P13, Motch et al. 2014) rather than IMBHs. It is actually interesting that the observations do not favour the 'simpler' resolution of this issue: the main difficulty with ULXs is that they should not radiate above the Eddington limit ($L_{\rm Edd} = 1.3 \times 10^{38} (M_{\rm X}/{\rm M}_{\odot})$ erg s^{-1}), and IMBHs with masses $M_{\rm X} \sim 10^2$–$10^4\,{\rm M}_{\odot}$ would remain comfortably below this limit.

A preliminary attempt to find pulsating ULXs (other than M82 X-2) in *XMM–Newton* archival data (Doroshenko, Santangelo & Ducci 2015) found none, but more sensitive surveys will follow. Our attention has turned to IC10 X-1 as an NS candidate because of its modest (for a ULX) luminosity ($L_{\rm X} \leq 1.2 \times 10^{38}$ erg s^{-1}) and its phase-shifted RV curve (Laycock et al. 2015). In such a case, the Corbet diagram (Corbet 1986) predicts the NS pulsations to lie in the $P_{\rm spin} < 1$ s range for the observed $P_{\rm orbit} = 1.45$ d. Notwithstanding the absence of any other known WR+NS binary, we suppose that such a system will lie between the supergiant (SG) and Roche-lobe overflow (RLOF) systems.

The lack of pulsations could plausibly be due to limitations of the current data sets. Time resolution in typical imaging mode for *Chandra* ACIS is 3.4 s, for *XMM–Newton* EPIC-MOS 2.6 s and for EPIC-PN 73 ms. The recent discovery of a 1.37 s pulsar in M82 X-2 by Bachetti et al. (2014) with *NuSTAR* shows that such objects can hide in plain sight if their spin periods lie below the timing threshold. At very short orbital periods (such as $P_{\rm orbit} = 1.45$ d for IC10 X-1 and $P_{\rm orbit} = 2.5$ d for M82 X-2), pulsations suffer Doppler blurring because of the orbital motion of the NS during an observation. The time required for the path length variation to accumulate a light-crossing time of $P_{\rm spin}/2$ and hence to go out of phase is $\delta t = c\,P_{\rm spin}/(2v_{\rm orbit})$, where c is the speed of light. This is as little as 250 s for the maximum projected velocity in Table 1 of $v_{\rm orbit} = 600$ km s^{-1} (Doppler shift $z = 0.004$). At the average uneclipsed *XMM–Newton* PN count rate of 0.5 counts s^{-1}, it will be challenging to detect such pulsations.

Stellar winds can wash out high-frequency variability when photons reaching the observer scatter off electrons lying at a wide range of distances from the NS (Kylafis & Klimis 1987). When the light-travel time across the scattering region is comparable to the pulse period, the modulation is lost. Assuming the scattering core of the WR wind to have a radius of $\leq 8\ {\rm R}_{\odot}$ (Table 1), pulse smearing would be significant for $P_{\rm spin} < 18$ s.

An NS with a magnetic field in the usual range for young objects (10^{12} G) should be a pulsar at IC10 X-1's accretion rate. The existence of a slow 7 mHz QPO (Pasham, Strohmayer & Mushotzky 2013) could then be attributed to the interaction of the magnetic field with the inner edge of the accretion disc. The type of QPO seen in IC10 X-1 is not BH-specific and occurs in many NS systems (Bozzo et al. 2009). It has long been known that high B-field NSs can switch off their pulsations and yet continue to emit X-rays. The best known example is A0538-66 which has been detected

on numerous occasions, but only once have pulsations been seen (Skinner et al. 1982). Magnetospheric accretion that is gated by rotational inhibition may also be able to create unpulsed emission. This mechanism has previously been invoked to explain the persistent low luminosity of some NS+Be systems in quiescence and as a way to turn off accretion in supergiant fast X-ray transients (SFXTs) where high mass-transfer rates are continuously present.

4 CONCLUSIONS

Based on a finding that the RV curve of the WR XRB IC10 X-1 is not phase-aligned with the X-ray eclipses, we have presented the case that the compact object in this system, rather than being a 20–30 $M_{\odot}$ BH, is an NS or a lower mass BH. If the RV curve is a projection of the WR's wind velocity, then there is no longer any *dynamical evidence* for a massive BH in IC10 X-1. In this Letter, we have focused on application of the van Kerkwijk et al. (1996) model for the interaction between the radiation field and the stellar wind in HMXBs, and we are keenly aware that the true picture is more complex. In summary, the weight of evidence points to a low mass compact object in X-1. A comparable interpretation for Cyg X-3 was explored by Zdziarski, Mikołajewska & Belczyński (2013). The wind velocity profile and spatial ionization structure remain unconstrained by observation, requiring higher resolution optical/IR spectra as input for modelling. The shape of the X-ray modulation is likely related to the scattering and absorption properties of the gas in the shielded sector which crosses the line of sight at mid-eclipse. Hard X-ray observations could probe the effects of scattering on the eclipse profile, while motivation for phase-resolved X-ray line spectra is established by Vilhu et al. (2009). The observed X-ray luminosity of X-1 (Wang et al. 2005) lies within the range exhibited by both NSs and stellar-mass BHs in HMXBs although it is substantially higher than most persistent NS+SG systems, and closer to the Be systems at the peaks of their giant outbursts. Super-Eddington luminosity has been seen in A0538-66 and recently in M82 X-2, so the possibility exists for an NS in IC10 X-1. The system is similar in many regards to other supposed BH-IMXBs which now should be examined closely with regard to the possibility that this phenomenon is more widespread.

ACKNOWLEDGEMENTS

This work was supported in part by NASA grant NNX14-AF77G.

REFERENCES

Bachetti M. et al., 2014, Nature, 514, 202
Barnard R., Clark J., Kolb U., 2008, A&A, 488, 697
Barnard R., Steiner J. F., Prestwich A. F., Stevens I. R., Clark J. S., Kolb U. C., 2014, ApJ, 792, 131
Belczynski K., Bulik T., Fryer C. L., 2010, ApJ, 714, 1217
Bogomazov A. I., 2014, Astron. Rep., 58, 126
Bozzo E., Stella L., Vietri M., Ghosh P., 2009, A&A, 493, 809
Bulik T., Belczynski K., Prestwich A., 2011, ApJ, 730, 140
Carpano S., Pollock A. M. T., Prestwich A., Kilgard R., Crowther P., Wilms J., Yungelson L., Ehle M., 2008, in Bandyopadhyay R. M., Wachter S., Gelino D., Gelino C. R., eds, AIP Conf. Proc. Vol. 1010, A Population Explosion: The Nature & Evolution of X-ray Binaries in Diverse Environments. Am. Inst. Phys., New York, p. 330
Casares J., Jonker P. G., 2014, Space Sci. Rev., 183, 223
Clark J. S., Crowther P. A., 2004, A&A, 414, L45
Corbet R. H. D., 1986, MNRAS, 220, 1047
Doroshenko V., Santangelo A., Ducci L., 2015, A&A, 579, A22
Farrell S. A. et al., 2014, MNRAS, 437, 1208
Feng H., Soria R., 2011, New Astron. Rev., 55, 166
Gilfanov M., Grimm H.-J., Sunyaev R., 2004, Nucl. Phys. B, 132, 369
Gladstone J. C., Roberts T. P., Done C., 2009, MNRAS, 397, 1836
Hanson M., Still M., Fender R., 2000, ApJ, 541, 308
Kylafis N. D., Klimis G. S., 1987, ApJ, 323, 678
Langer N., 1989, A&A, 210, 93
Laycock S. G. T., Cappallo R. C., Moro M. J., 2015, MNRAS, 436, 1399
Liu J.-F., Bregman J. N., Bai Y., Justham S., Crowther P., 2013, Nature, 503, 500
Luangtip W., Roberts T., Mineo S., Lehmer B., Alexander D., 2014, in Ness J.-U., ed., The X-ray Universe 2014, p. 120
Maccarone T. J., Lehmer B. D., Leyder J. C., Antoniou V., Hornschemeier A., Ptak A., Wik D., Zezas A., 2014, MNRAS, 439, 3064
Medvedev A. S., Poutanen J., 2013, MNRAS, 431, 2690
Motch C., Pakull M. W., Soria R., Grisé F., Pietrzynski G., 2014, Nature, 514, 198
Park K., Ricotti M., 2011, ApJ, 739, 2
Pasham D. R., Strohmayer T. E., Mushotzky R. F., 2013, ApJ, 771, L44
Prestwich A. H. et al., 2007, ApJ, 669, L21
Remillard R. A., McClintock J. E., 2006, ARA&A, 44, 49
Silverman J., Filippenko A., 2008, ApJ, 678, L17
Skinner G. K., Bedford D. K., Elsner R. F., Leahy D., Weisskopf M. C., Grindlay J., 1982, Nature, 297, 568
Soria R., 2007, in Karas V., Matt G., eds, Proc. IAU Symp. 238, Black Holes from Stars to Galaxies – Across the Range of Masses. Cambridge Univ. Press, Cambridge, p. 235
Stella L., White N. E., Rosner R., 1988, ApJ, 308, 669
Tutukov A. V., Fedorova A. V., Cherepashchuk A. M., 2013, Astron. Rep., 57, 657
van Kerkwijk M. H., Geballe T. R., King D. L., van der Klis M., van Paradijs J., 1996, A&A, 314, 52
Vilhu O., Hakala P., Hannikainen D. C., McCollough M., Koljonen K., 2009, A&A, 501, 679
Wang Q. D., Whitaker K. E., Williams R., 2005, MNRAS, 362, 1065
Zdziarski A. A., Mikołajewska J., Belczyński K., 2013, MNRAS, 429, L104

This paper has been typeset from a TEX/LATEX file prepared by the author.